Fuel 364 (2024) 131102

Contents lists available at ScienceDirect

Fuel

journal homepage: www.elsevier.com/locate/fuel

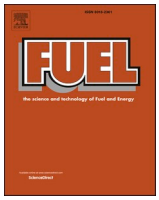

Full Length Article

Reaction pathways of phenol steam reforming over Rh and Ni-Co based catalysts supported on γ-Al_2O_3

Marinela D. Zhurka [a], Alan J. McCue [b], Panagiotis N. Kechagiopoulos [a,*]

[a] Chemical Processes & Materials Group, School of Engineering, University of Aberdeen, Aberdeen AB24 3UE, UK
[b] Advanced Centre for Energy and Sustainability (ACES), Department of Chemistry, School of Natural and Computing Sciences, University of Aberdeen, Aberdeen AB24 3UE, Scotland, UK

ARTICLE INFO

Keywords:
Phenol steam reforming
Hydrogen production
Nickel
Cobalt
Rhodium
Reaction pathway

ABSTRACT

Phenol steam reforming is an attractive method for the sustainable production of hydrogen. Phenol can be found in wastewaters from the textiles and pharmaceutical industries and is further contained at high concentrations in bio-oils and tars derived from biomass pyrolysis and gasification. Despite a range of studies reporting on optimal catalysts for the reaction, respective reaction pathways have been comparatively discussed in less detail. In the current work we present a detailed kinetic study of the steam reforming of phenol over Rh and Ni-Co catalysts supported on γ-Al_2O_3. The effect of temperature, partial pressure of reactants, and contact time is studied to propose a reaction mechanism over the catalysts. Results suggest that initial reaction pathways are affected by the oxophilicity of the metal. Over Rh, phenoxy formation via O-H bond cleavage is prominent, while over Ni-Co, C-O bond scission appears to be dominant due to the presence of Co and its affinity to oxygen. Due to these kinetic features, the selectivity to benzene is pronounced over Ni-Co in contrast to Rh, while CO is found to be a secondary product on the bimetallic catalyst unlike the noble metal one. Across the range of conditions studied, Rh achieved higher conversion, hydrogen yield and higher stability as a result of significantly lower carbon formation as demonstrated via time-on-stream experiments and analysis of coke deposits on spent catalyst samples.

1. Introduction

Among renewable resources, lignocellulosic biomass is particularly suited as an abundant, low-cost feedstock for the production of bio-based chemicals, fuels and energy to substitute fossil resources. Bio-oil, the liquid product of biomass pyrolysis, can be steam reformed to produce hydrogen, the latter utilised as an energy carrier or used to further upgrade bio-oils to fuels and chemicals through hydro-deoxygenation [1,2]. Similarly, tars, the volatile products of gasification, need to be steam reformed, in situ or downstream, to enhance the efficiency of the process [3–5]. Despite extensive research on hydrogen production from steam reforming of aliphatic oxygenates, the conversion of aromatic oxygenated compounds by steam reforming has been studied less due to challenges related to high deactivation rates and coking [2,6].

Phenol Steam Reforming (PSR) is an attractive method to sustainably produce hydrogen. Phenol is contained in high concentrations in bio-oil and tars [7] and can be considered a model compound of their aromatic fraction. Moreover, it can be found in industrial wastewater from the textiles [8] and pharmaceuticals industries [9]. The desired products are H_2 and CO_2 according to the overall reaction (1) (Table 1), with hydrogen production further influenced by the water gas shift (WGS) reaction (2). However, in practise various reactions (3) to (9) occur in parallel, yielding products such as methane, carbon monoxide, benzene, naphthalene, and coke.

A range of studies have reported on optimal catalysts and operating conditions for the phenol steam reforming reaction [10–12] or focused on catalyst deactivation due to coking [13,14]. Ni based catalysts have been widely studied due to the metal's high activity and low cost [11,13–19], however extensive coking remains a major issue on the metal. Noble metals, in particular Rh, exhibit much higher activity and coking resistance, a feature well documented in a range of reforming applications, including PSR [20]. Ni-Rh catalysts have been studied too for the PSR reaction to combine the benefits of both metals at a reduced cost [21]. Cobalt has also attracted research interest for PSR due to its lower cost in comparison to noble metals and higher coking resistance in

* Corresponding author.
E-mail address: p.kechagiopoulos@abdn.ac.uk (P.N. Kechagiopoulos).

https://doi.org/10.1016/j.fuel.2024.131102
Received 17 October 2023; Received in revised form 15 January 2024; Accepted 26 January 2024

Table 1
Phenol steam reforming main reactions [13,17,27,28].

Overall steam reforming	$C_6H_5OH + 11H_2O \rightleftarrows 14H_2 + 6CO_2$	(1)
Water gas shift	$CO + H_2O \rightleftarrows CO_2 + H_2$	(2)
Phenol decarbonylation	$C_6H_5OH \rightleftarrows C_5H_6 + CO$	(3)
Phenol hydrodeoxygenation	$C_6H_5OH + H_2 \rightleftarrows C_6H_6 + H_2O$	(4)
Phenol decomposition	$C_6H_5OH + 4H_2O \rightleftarrows 3.5CH_4 + 2.5CO_2$	(5)
Naphthalene formation	$2C_5H_6 \rightleftarrows C_{10}H_8 + 2H_2$	(6)
Methanation	$CO + 3H_2 \rightleftarrows CH_4 + H_2O$	(7)
Benzene polymerisation	$C_6H_6 \rightarrow C_{polymers}$	(8)
Naphthalene polymerization	$C_{10}H_8 \rightarrow C_{polymers}$	(9)

comparison to Ni [22,23]. In this regard, Ni-Co bimetallic catalysts shown to possess enhanced C-H bond breaking ability in other hydrocarbon reforming reactions [24], have been recently studied, exhibiting promising performance and stability [10,25,26].

Despite advances in catalyst design for PSR, significantly fewer studies have discussed in detail the reaction pathways of the process. Depending on catalyst and operating conditions, phenol decomposition has been proposed to initiate via O-H and C-O bond scission followed by the aromatic ring opening, resulting in H_2, CO and C_xH_y species [16]. C-H and C-C bond scission have also been discussed as first steps, leading to adsorbed hydrocarbon fragments which react with hydroxyl groups to produce CO_x and H_2 [20]. An experimental study of phenol decomposition on Ni suggested that O-H bond cleavage was more likely to occur than the C-O bond scission leading to phenoxy species formation [27]. The mechanism proposed involved the extraction of intact CO from the phenoxy species via C-C bond rupture. Direct dehydroxylation of phenol has also been observed on Ni based catalysts, forming benzene which upon decomposition led to significant CH_4 formation [28]. Phenol hydrodeoxygenation to benzene (4) is observed at low operating temperatures [17], while phenol decarbonylation (3) is favoured at high operating temperatures. The latter results in the formation of cyclopentadiene, which is a naphthalene precursor (6) [13]. The reactivity of phenol on Rh has been previously examined given the metal's excellent catalytic activity in reforming reactions and coking resistance. Results indicated that at low temperatures phenoxy species formation via O-H bond cleavage was favoured, followed by the C-O bond scission [29]. At high operating temperatures phenol selectively decomposed to various carbonaceous products [29]. DFT calculations on the dissociation of phenol on Rh surfaces suggested that phenol could dissociatively adsorb with the aromatic ring parallel to the surface forming phenoxy species [30] or directly deoxygenate via C-O bond cleavage, yielding benzene [31]. DRIFTS experiments of phenol decomposition suggested that the oxophilic sites of Co were responsible for the direct dehydroxylation of phenol followed by further decomposition of the intermediate formed species, such as benzene [28].

The present work focuses on the detailed kinetic study of the steam reforming of phenol, examined in a fixed-bed reactor over Rh and Ni-Co catalysts. The effect of temperature, partial pressure of reactants, contact time and metal is investigated to elucidate on reaction pathways and propose a reaction mechanism over the catalysts.

2. Methodology

2.1. Catalysts preparation

The catalysts used in this work were prepared via the wet impregnation method. Rhodium and nickel–cobalt catalysts were prepared using $RhCl_3{\cdot}3H_2O$ (Pressure Chemical), $Ni(NO_3)_2{\cdot}6H_2O$ (Merck) and $Co(NO_3)_2{\cdot}6H_2O$ (Merck) as precursors to obtain metal loadings of 0.7 wt% for the Rh catalyst and 10 wt% (Ni/Co = 1) for the Ni-Co catalyst.). γ-Al_2O_3 (Alfa Aesar, Catalog no. 43832, catalyst support, high surface area, bimodal) provided in 1/8″ pellets was ground and sieved to obtain a particle size of 250–355 μm, used as support. The aqueous solution of the metal precursor(s) was mixed with the support particles and stirred for 1 h at 80 °C. The solvent was removed via evaporation under mild vacuum conditions followed by drying overnight at 110 °C. The Rh catalyst was subsequently calcined in air flow at 600 °C for 5 h, while the Ni-Co catalyst was calcined at 700 °C for the same duration.

2.2. Characterization of fresh and spent catalysts

Rh, Ni and Co content of the obtained catalysts was determined by inductively coupled plasma-optical emission spectroscopy (ICP-OES) elemental analyses carried out after dissolution of the samples by acid digestion on a Varian 720ES ICP-OES at Medac Ltd, UK. Temperature Programmed Reduction (TPR) experiments on fresh oxidised samples as obtained after calcination were conducted to characterize the metal surface of the catalyst and investigate the optimal reduction conditions. A TPDRO 1100 instrument was used with a TCD detector, with a trap bed placed before the detector to remove the moisture. Samples were firstly dried by increasing the temperature up to 200 °C for 30 min under N_2 flow, then the system was cooled down and the temperature was increased again until 800 °C with a 10 °C min^{-1} temperature ramp, using a 5 % H_2/N_2 flow. XRD patterns were obtained at room temperature on a Panalytical powder diffractometer to identify crystalline phases present. The diffraction patterns were recorded over an angular range of $10° < 2\theta < 90°$ with a step-size of 0.013°. Temperature Programmed Oxidation (TPO) analysis was used to qualitatively and quantitatively characterise carbon deposits on spent catalyst samples, performed in situ following time-on-stream experiments in the same experimental setup used for the kinetic testing (see below). Spent catalyst samples were pre-treated in a N_2 flow at 250 °C for 30 min and then allowed to cool to room temperature. The temperature was subsequently increased to 750 °C at a rate of 5 °C min^{-1} under a 10 % O_2/N_2 flow of 60 NmL min^{-1}. Product outlet composition was monitored to quantify the CO_2 evolution and subsequently calculate the total carbon content deposited.

2.3. Reactor setup

The kinetic study took place in a fully automated, computer-controlled reaction system by PID Eng & Tech (Micro Activity-Effi unit). An HPLC pump (Gilson 307) was used to deliver the reactants feed (phenol and water). The feed was channelled at appropriate residence time through the hot box of the unit, operating at 180 °C, to ensure its vaporisation. The vapours were subsequently mixed with N_2, fed via a mass flow controller (Bronkhorst El-Flow Select), with N_2 also used as an internal standard during gas product analysis via gas chromatography. Reaction products exiting the hot box were fed into a gas/liquid separator, operated at 0 °C, where condensables were separated and collected. Analysis of the gas products took place on-line via a HP5890 GC equipped with a Thermal Conductivity Detector (TCD) and MS–5A and HS–T packed columns, while liquids were analysed off-line in a Perkin-Elmer GC equipped with a Flame Ionisation Detector (FID) and a CP 7502 CP-Chirasil Dex CB capillary column. Details on calibration procedures and method details of the GC analysis of gas and liquid products are provided in Section S2.1 in the Supporting Information (SI).

2.4. Experimental conditions and parameters

Prior to each experiment the catalyst was reduced using a flow of 5 % H_2 in N_2 for 1 h at 600 °C (determined via TPR as a sufficient reduction temperature for both catalysts). Reaction temperature was varied from 450 °C to 700 °C at total pressure of 1.9 bar under various Steam/Carbon (S/C) ratios (2–9 mol_{H2O} mol_C^{-1}). The space time effect was examined by varying the feed flow from 88 to 240 NmL min^{-1}, with a S/C ratio of 2 or 7, over a fixed catalyst mass ($W/F_{t0,Ph}$ from 59 to 290 g_{cat} s g_{Ph}^{-1}) at 600 °C, under a steady pressure of 1.8 bar. All pressures reported refer to absolute values. The partial pressure of water was varied from 0.52 to

1.82 bar at constant total pressure of 1.9 bar and partial pressure of phenol (0.04 bar). Correspondingly, the partial pressure of the phenol was varied from 0.03 to 0.11 bar at constant total pressure of 1.9 bar and partial pressure of water (1.35 bar). Partial pressure variation experiments were carried out at 600 °C. Stability runs (time-on-stream effect) on phenol steam reforming were carried out at 500 °C and S/C of 2, running for 3 h at a space time of 263 g_{cat} s g_{Ph}^{-1}. A mass of 50 mg catalyst was used in all experiments, except the space time runs where 30 mg of catalyst were used. Table S1 in the SI details the experimental conditions studied and respective values of all operating parameters.

Multiple tests were carried out at the same conditions to verify the repeatability of results, while at the start and end of every experimental session the performance of the catalyst was evaluated at reference conditions to ensure significant deactivation had not occurred. For each variable variation experiment, data were collected across a minimum of two distinct reaction runs (one run testing condition 1, 3, and 5 in increasing order, and a second run testing condition 6, 4 and 2 in decreasing order) to ensure the consistency of trends. For each experimental condition, at least three consecutive samples were collected across a time frame of 40–60 min to ensure the stable operation at the respective conditions. Atomic C, H and O mass balance closure in all tests was in the order of 100 ± 5 %, whereas conversion and selectivity error margins were below 2 %. The results presented in following sections, based on the overall phenol steam reforming reaction (1), are expressed in terms of the following parameters, where $F_i^{in/out}$ is the inlet/outlet molar flow of compound i (mol s^{-1}):

Conversion of phenol (%): $X = \frac{F_{Ph}^{in} - F_{Ph}^{out}}{F_{Ph}^{in}} \times 100$

Carbon selectivity of product compound y with n carbon atoms: $S_c(y) = \frac{n \cdot F_y}{6 \cdot (F_{Ph}^{in} - F_{Ph}^{out})} \times 100$

Hydrogen yield: $Y_{H_2} = \frac{F_{H_2}^{out}}{14 \cdot F_{Ph}^{in}} \times 100$

Intrinsic phenol conversion rates were defined based on the nominal metal content according to the below equation:

$$r_{Ph}(s^{-1}) = \frac{X_{Ph} \cdot F_{Ph}^{in} \cdot AW_m}{w_{cat} \cdot w_m}$$

where w_{cat} is the catalyst weight, w_m the actual weight composition of Rh (0.52 %) or Ni (5.71 %) and Co (5.87 %) determined by ICP-OES, and AW_m the atomic weight of metal, which in the case of the Ni-Co is weighted based on the individual loadings of the two metals.

3. Experimental results

3.1. Catalysts characterization

3.1.1. Temperature-programmed reduction (H_2-TPR)

The reducibility of both calcined catalysts was investigated by H_2 temperature-programmed reduction (H_2-TPR), and the profiles are presented in Fig. 1. Regarding the Ni-Co catalyst, two H_2 consumption peaks are observed. The first peak at temperatures below 450 °C is ascribed to the reduction of Ni and Co simple oxides to Ni^0 and Co^{2+} [32]. The second peak at temperatures over 450 °C is attributed to the reduction of the remaining Co^{2+} to Co^0, the reduction of Ni^{2+} species strongly interacting with the support [33] and the reduction of spinel oxides [34,35]. Usually, the reduction of Ni and Co oxides would be expected to occur at different temperatures, however only single reduction peaks at 350 °C and 510 °C are visible. This suggests that Ni and Co form mixed oxides ($NiO/Ni_xCo_{1-x}O$ and $Co_3O_4/NiCo_2O_4$) providing an easier way for the formation of Ni-Co alloy during reduction [36] (further discussed in the XRD profile below). Considering that $NiAl_2O_4$ and $CoAl_2O_4$ reduction takes place above 800 °C [32,37], their formation can be excluded. For the Rh based catalyst, the peaks at 120 °C and 130 °C are attributed to the reduction of surface Rh_xO_y to Rh, while peaks above 150 °C are assigned to the reduction of RhO_yCl_z species, which were formed through the oxidation of the $RhCl_3$ precursor during calcination [38,39]. The broad peak observed at 400 °C is attributed to the reduction of $RhAl_xO_y$, which could be formed at the metal-support interface by diffusion of Rh_xO_y into the alumina, indicating a strong metal-support interaction [40]. Finally, the small peak at 610 °C indicates a high chemical stability and could possibly be attributed to the reduction of rhodium aluminate ($Rh(AlO_2)_y$) [41]. Nonetheless, it has also been discussed in literature that γ-Al_2O_3 can incorporate chloride into its structure [42,43]. The complete removal of chloride requires temperatures higher than 600 °C [44], so signal evolution could possibly be also related to residual chloride reduction.

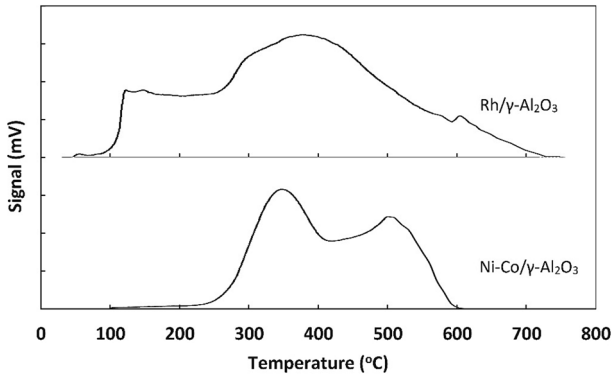

Fig. 1. Temperature-programmed reduction (TPR) profiles of calcined Rh/γ-Al_2O_3 and Ni-Co/γ-Al_2O_3 catalysts.

3.1.2. X-ray diffraction (XRD)

X-ray diffractogram were analysed based on reference data for γ-Al_2O_3 [45], Co_3O_4 [46], $CoAl_2O_4$ [47], $NiAl_2O_4$ [48], $NiCo_2O_4$ [49], NiO [50], Rh_2O_3 [51] and RhO_2 [52], compiled in Section S2.3, Figure S4, in the SI. The diffractogram for the calcined Rh catalyst is shown in Fig. 2, however, due to the low content of Rh, no Rh_xO_y peaks were detected. Peaks characteristic of the γ-Al_2O_3 support are visible at 37°, 46° and 67° 2θ [39,53]. Equivalent peaks due to the γ-Al_2O_3 support are present in the XRD patterns of the calcined Ni-Co catalyst. As can be seen in Figure S4, Co_3O_4, $CoAl_2O_4$, $NiAl_2O_4$ and $NiCo_2O_4$ are difficult to distinguish by XRD, as their reflections largely overlap. Considering the TPR results that excluded the formation $NiAl_2O_4$ and $CoAl_2O_4$, the peak at 19° 2θ is attributed to the presence of Co_3O_4, while the peak at 31° 2θ indicates the presence of $NiCo_2O_4$ and Co_3O_4 phases. The intensity of the peak at 37° 2θ is likely a combination of γ-Al_2O_3 and Ni-Co phases, namely Co_3O_4, $NiCo_2O_4$ and NiO. Peaks at 45° and 46.5° 2θ indicate γ-Al_2O_3 and NiO phases. The peak at 59° 2θ is attributed to $NiCo_2O_4$ and Co_3O_4 phases. Finally, the peaks at 65° and 66° 2θ are ascribed to the presence of γ-Al_2O_3, Co_3O_4, and $NiCo_2O_4$ [54,55]. It is possible that

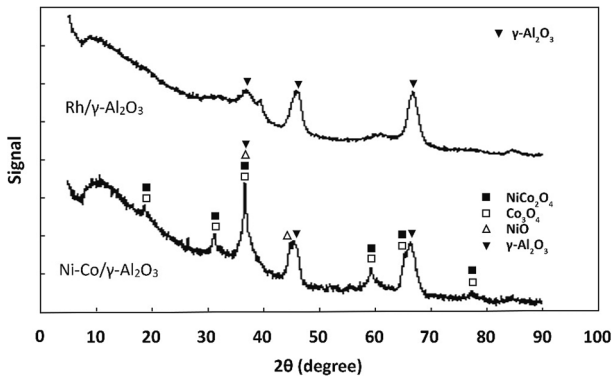

Fig. 2. X-ray diffractograms of calcined Rh/γ-Al_2O_3 and Ni-Co/γ-Al_2O_3 catalysts. Fig. S4 in the SI presents detailed X-ray diffraction reference data.

peaks attributed to NiO are partly due to the presence of a $Ni_xCo_{1-x}O$ solid solution [33]. The identification of the latter is challenging as its peaks overlap with those of NiO [33], however its formation has been shown to be enhanced at calcination temperatures higher than 350 °C [56]. Considering a calcination temperature of 700 °C was applied for the Ni-Co catalyst, the $Ni_xCo_{1-x}O$ and subsequent Ni-Co alloy formation upon reduction can be expected. These results for the bimetallic catalyst are in agreement with the TPR profile where the presence of single reduction peaks both at low temperature (simple oxides) and high temperature (oxides strongly interacting with support and spinels) indicated the formation of Ni-Co alloy upon reduction.

3.2. Effect of temperature

Fig. 3 shows the effect of temperature on the conversion of phenol and H_2 yield at different S/C ratios and catalysts. On the Rh catalyst, increasing the temperature from 450 °C to 700 °C leads to the increase of phenol's conversion from 9 % to 26 % at S/C = 2 and from 14 % to 53 % at S/C = 9. H_2 yield follows conversion's trend, reaching 13 % and 31 % for S/C of 2 and 9, respectively, at 700 °C. Similar trends are observed on the Ni-Co catalyst, with conversion increasing from 3 % to 17 % at S/C = 2 and from 5 % to 42 % at S/C = 9. H_2 yield over Ni-Co equivalently reaches 5 % and 18 % for S/C of 2 and 9, respectively, at 700 °C. Across the range of conditions studied, the Rh catalyst shows higher catalytic activity than the bimetallic Ni-Co catalyst.

The carbon selectivities of the products are presented in Fig. 4. For both catalysts, gas phase products primarily consisted of CO and CO_2 (panels (a) to (d)), while liquid products contained mainly benzene and naphthalene (panels (e) to (h)). Traces of CH_4, C_2H_2 and C_3H_6 were also present in the gas product stream but below quantification limits, in agreement with tar steam reforming studies over Ni and Rh catalysts reporting no significant methane [18], acetylene [57] and propylene

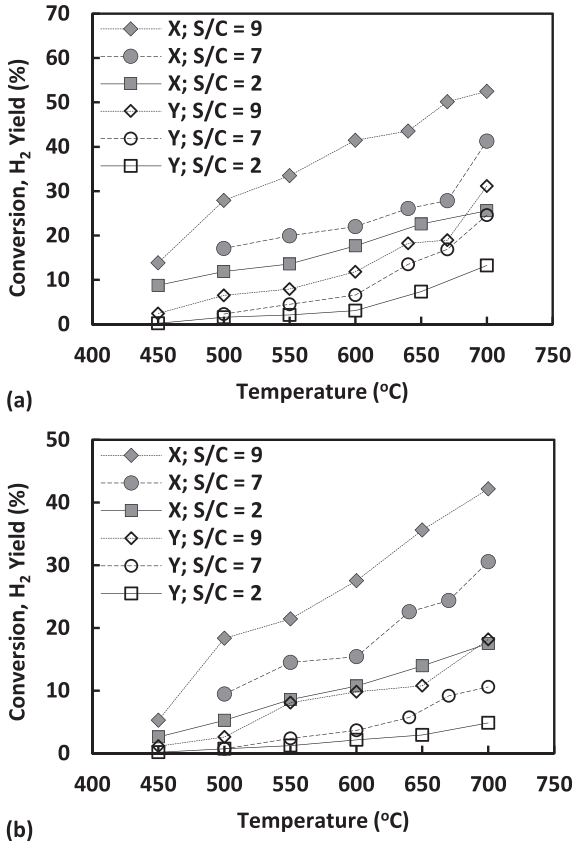

Fig. 3. Temperature effect on phenol conversion (X) and H_2 yield (Y) on Rh (a) and Ni-Co (b) catalysts (W/F_{Ph} = 50 g_{cat} s g_{Ph}^{-1}, P = 1.9 bar, S/C = 2–9).

[58] production above 500 °C. Thermodynamic equilibrium predicts substantial methane formation, especially at temperatures below 550 °C and S/C ≤ 5 (Figure S1, SI), indicative of the experimental results being under kinetic control and both catalysts being able to efficiently reform CH_x fragments. A high CO selectivity is observed on both catalysts at 450 °C and S/C = 2 (67 % and 62 % on Rh and Ni-Co, respectively), indicating that decarbonylation reactions are favoured at these operating conditions. When increasing the S/C ratio, lower CO and higher CO_2 selectivities are observed, with CO_2 selectivity at 450 °C increasing from 20 % (S/C = 2) to 48 % (S/C = 9) on Rh, and from 11 % (S/C = 2) to 31 % (S/C = 9) on Ni-Co. This is in line with an expected promotion of the WGS reaction due to the abundance of steam. Increase of temperature is also seen to enhance kinetically the WGS reaction, as indicated by the decreasing trend of CO and concurrent rise of CO_2 (Fig. 4) and H_2 (Fig. 3). At 700 °C and S/C of 9, CO selectivity drops below 7 % on Rh and 12 % on Ni-Co, with the respective CO_2 selectivity values surpassing 87 % on Rh and 81 % on Ni-Co. The CO/CO_2 ratio in the products for S/C = 2 decreases from 3.24 to 0.55 on Rh and from 5.63 to 0.92 on Ni-Co with temperature rise from 450 °C to 700 °C, whereas the respective equilibrium value increases from 0.04 to 1.21 (Figure S1 panels (a) and (b), SI). Similarly, at S/C of 9 and from 450 °C to 700 °C, the CO/CO_2 ratio decreases from 0.92 to 0.08 on Rh and from 1.45 to 0.14 on Ni–Co, with the respective equilibrium value ranging from 0.24 to 0.18 (Figure S1 panels (a) and (b), SI). At the lower temperatures the WGS reaction is highly non-equilibrated over both catalysts, with the reaction approaching equilibrium at 650 °C and above. Nonetheless, the Rh based catalyst exhibits higher WGS activity, with CO/CO_2 ratio values achieved being almost half to those over the Ni-Co catalyst across the temperature range studied.

For both catalysts, benzene (Fig. 4 panels (e) and (f)) is an important product, resulting from the C-O bond cleavage of phenol or surface phenoxy groups and subsequent hydrogenation of formed phenyl species. A high selectivity (12 % on Rh and 25 % on Ni-Co) at 450 °C and S/C of 2 is observed, however, promotion of reforming and decomposition reactions with increasing temperature results in a decrease of this value for both catalysts (3.5 % on Rh and 5 % on Ni-Co at 700 °C). Benzene selectivity also decreases with increasing S/C for the whole temperature range, reaching values close to zero at the highest temperature and S/C on both catalysts, in agreement with a promotion of reforming reactions by excess steam. According to thermodynamic equilibrium, benzene production occurs only during phenol decomposition in the absence of steam (Figure S2, SI), with no benzene formed even at a S/C = 1, which is below PSR stoichiometry (Figure S1, SI). Comparing the two catalysts at similar conversions, a higher benzene selectivity is observed on the Ni-Co catalyst at temperatures below 600 °C. At S/C = 2 and conversions 9 % (T = 450 °C), 11 % (T = 500 °C) and 14 % (T = 550 °C), benzene selectivity on Rh was approximately 12 %, 11 % and 9 %, respectively, while on Ni-Co selectivity values of 19 % (T = 550 °C), 14 % (T = 600 °C) and 9 % (T = 650 °C) were obtained. These findings, as will be discussed in more detail below, could be attributed to the higher oxophilicity of Co in comparison to Rh [59,60] and the high affinity of Co to the O atom in the OH group of phenol. Results are in line with prior anisole hydrodeoxygenation (HDO) studies having suggested the more oxophilic metals to be responsible for direct C-O bond cleavage, favouring benzene formation [61]. Lastly, it should be noted that the same conversions occur at different operating temperatures with the Ni-Co catalyst requiring higher operating temperatures than Rh to achieve the same conversion value at a certain S/C.

Naphthalene (Fig. 4 panels (g) and (h)) was also detected in the liquid products over both catalysts. Thermodynamic equilibrium again predicts naphthalene production only during phenol decomposition (Figure S2, SI). Experimentally, higher selectivity values were observed with increasing temperature and decreasing S/C ratio (highest values of 14 % and 10 % observed on Rh and Ni-Co, respectively, at 700 °C and S/C = 2). When increasing the S/C ratio above 7 at 700 °C, naphthalene selectivity decreased to 5 % and 7 % on Rh and Ni-Co, respectively,

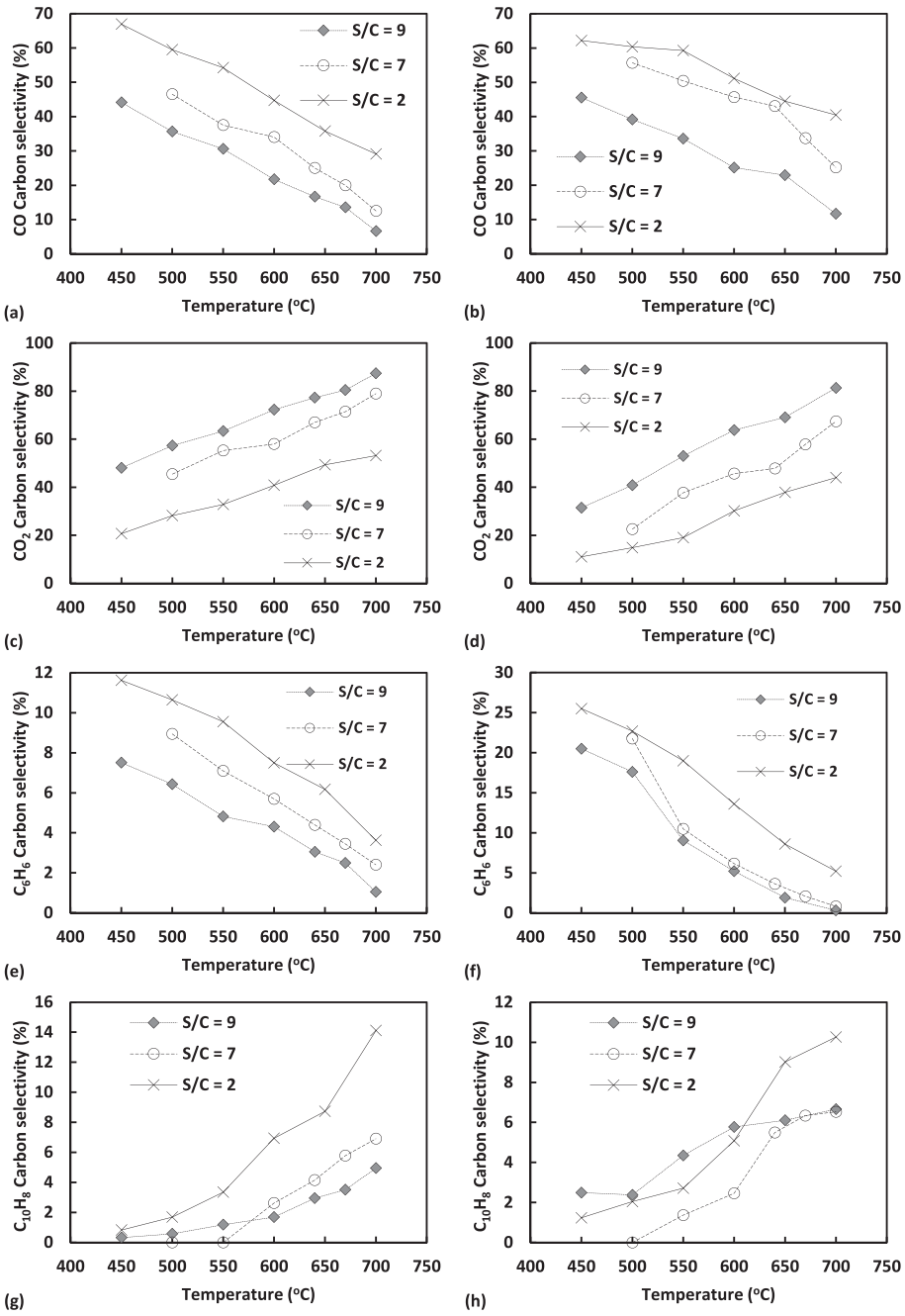

Fig. 4. Temperature effect on carbon selectivities of CO, CO_2, C_6H_6 and $C_{10}H_8$ on Rh (left column) and Ni-Co (right column) catalysts ($W/F_{Ph} = 50\ g_{cat}\ s\ g_{Ph}^{-1}$, P = 1.9 bar, S/C = 2–9).

evidencing that the addition of steam prevents the formation of naphthalene through reforming of the compound's precursors. As with benzene, at the same conversion, the Ni-Co catalysts shows higher naphthalene selectivity in comparison to Rh. At a conversion of 28 % (T = 500 °C, S/C = 9), 22 % (T = 600 °C, S/C = 7) and 14 % (T = 550 °C, S/C = 2) selectivity of 0.6 %, 2.6 % and 3.4 % were obtained on Rh, while on Ni-Co catalyst at the same conversions and respective S/C ratios selectivity values were 5.8 % (T = 600 °C), 5.5 % (T = 640 °C) and 9.0 % (T = 650 °C). It is noted again that Ni-Co requires higher operating temperature to achieve the same conversion as Rh. Overall, results indicate that naphthalene's formation is driven by temperature that promotes the decomposition of the aromatic ring and the subsequent coupling/recombination of its derivatives, in line with prior gas phase studies [62].

3.3. Variation of phenol partial pressure

The effect of phenol partial pressure on phenol conversion and H_2 yield is presented in Fig. 5a as a function of S/C ratio, with the equivalent partial pressures of phenol also annotated. During these experiments, according to procedures applied in Wei and Iglesia [63], the total inlet flow (210 NmL min^{-1}), partial pressure of water (1.35 bar), and total pressure (1.9 bar) were kept constant while varying the partial pressure of phenol from 0.03 to 0.11 bar (balanced by N_2), which corresponded to a S/C variation from 7 to 2. For both catalysts, the conversion increased with the S/C ratio, from 9 % to 26 % for Rh and from 5 % to 16 % for Ni-Co, with H_2 yield reaching 14 % on Rh and 7 % on Ni-Co at the highest S/C. As has been discussed in steam reforming literature [64], rates are affected negatively by the increase of the flowrate of

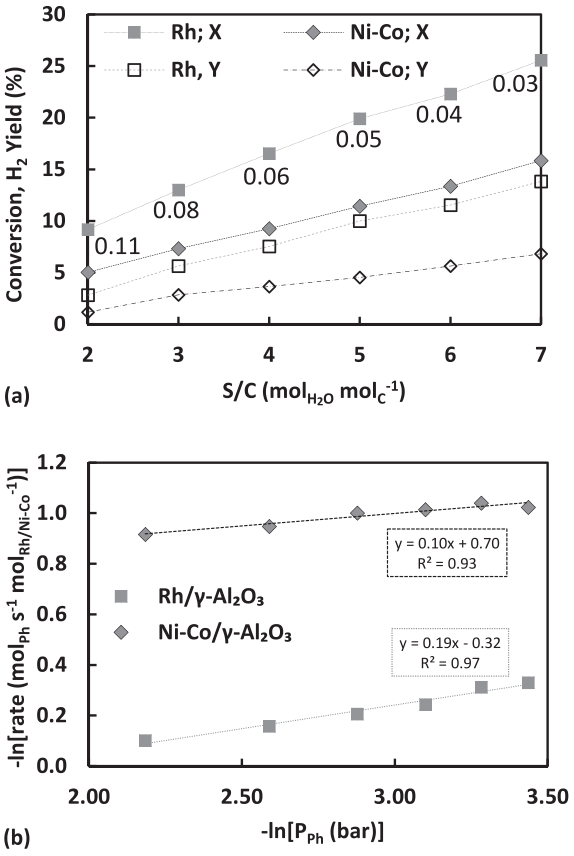

Fig. 5. Phenol partial pressure effect on phenol conversion (X) and H_2 yield (Y) on Rh and Ni-Co catalysts presented as a S/C variation with numbers on plot annotating the equivalent partial pressures of phenol in bar (a), and reaction order of PSR with respect to phenol partial pressures at 600 °C (b) (P = 1.9 bar, Q_{tot} = 210 NmL min^{-1}).

the primary reactant at constant total space velocity, and, conversely, positively, by the increase of its partial pressure. The observed increase in conversion is linked to the decreasing flow of phenol at a constant total space time applied in these experiments. Conversion and H_2 yield over the Rh catalyst are almost double to those over Ni-Co, in line with the observations in the previous section. A positive reaction order in phenol partial pressure equal to 0.19 and 0.1 for Rh and Ni-Co, respectively, is observed (Fig. 5b), suggesting the participation of a phenol derived surface intermediate in the rate determining step. Evidently, the increase in partial pressure promotes the conversion of phenol, despite the decrease in conversion that is obtained due to the increasing flow of phenol. The low reaction order values could indicate the strong adsorption of the aromatic on the catalyst surface. Indicatively, DFT calculations predicted the strong adsorption of phenol over Rh(1 1 1) at a high binding energy of 2.79 eV, with the aromatic ring adsorbing parallel to the catalyst surface [30]. The lower reaction order on Ni-Co could be linked to the increased presence of benzene on that catalyst compared to Rh. Benzene adsorption on a range of metals has been calculated to be stronger than that of oxygenated aromatics over the same catalyst (e.g., benzene versus phenol on Ni(1 1 1) [65] or Pd (1 1 1) [66], and benzene versus anisole on Pt(1 1 1) [67]), hence its increased presence on the catalyst could be hindering the conversion of phenol.

The carbon selectivities of the products in terms of S/C variation are presented on Fig. 6. Relatively high selectivities for CO (36 % and 53 % for Rh and Ni-Co, respectively) and CO_2 (51 % and 31 % for Rh and Ni-Co, respectively) are obtained for S/C = 2, in line with the results at 600 °C presented in the previous section. Increasing the S/C ratio to 7, the WGS reaction is further enhanced with CO_2 selectivity reaching 70 % on Rh and 42 % on Ni-Co, and CO selectivity decreasing to 23 % and 47 %, respectively. The selectivity of C_6H_6 decreases with increasing S/C from 7 % to 3 % on Rh and from 8 % to 6 % on Ni-Co. A similar trend is observed for $C_{10}H_8$ with its selectivity decreasing from 7 % to approximately 4 % on both catalysts. The results suggest that dehydroxylation and decarbonylation reactions, involving C-O and C-C bond cleavages, are dominant at low S/C ratios, while reforming and WGS reactions are enhanced at high S/C ratios. Naphthalene's selectivity is similar on both catalysts, suggesting again the primary impact of temperature on its

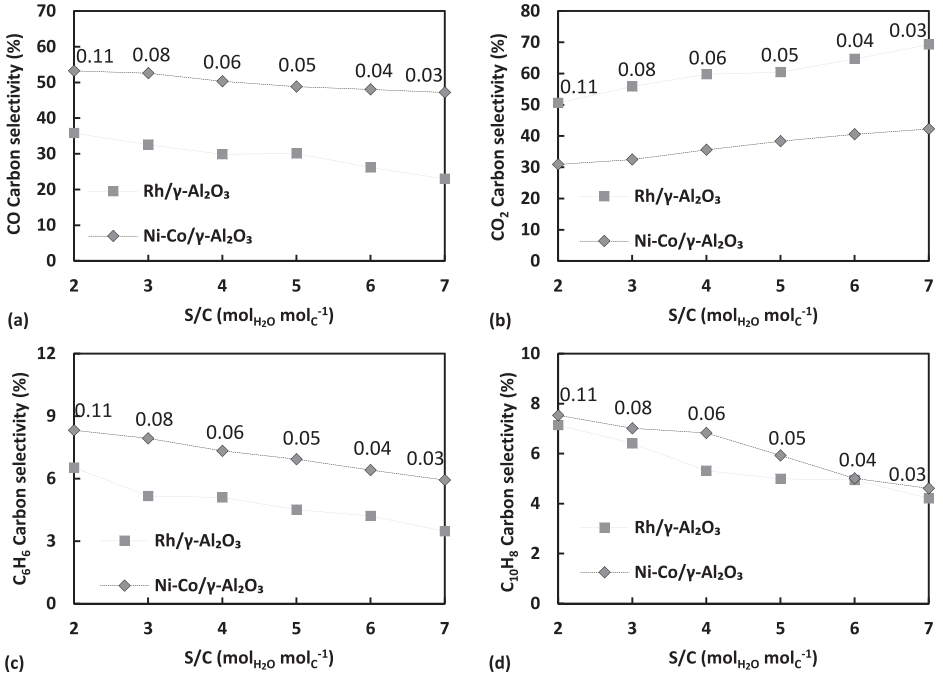

Fig. 6. Phenol partial pressure effect on carbon selectivities of CO (a), CO_2 (b), C_6H_6 (c) and $C_{10}H_8$ (d) on Rh and Ni-Co catalysts at 600 °C presented as a S/C variation with numbers on plot annotating the equivalent partial pressures of phenol in bar (P = 1.9 bar, Q_{tot} = 210 NmL min^{-1}).

formation. Acid sites on the γ-Al_2O_3 support could also be favouring phenol's decomposition via tautomerization reactions, which have been previously shown to be promoted on Lewis acid sites [68]. To test this, phenol reforming and decomposition over γ-Al_2O_3 alone at a temperature range of 500 °C to 700 °C was carried out. These experiments were not quantitative due to challenges related to minimal production of gas products and evaporating and feeding consistently pure phenol (for decomposition runs), however qualitatively only naphthalene and to a lesser extent benzene were detected above 650 °C. No products were formed at lower temperatures, suggesting an overall reduced role of the support at the studied conditions.

3.4. Variation of water partial pressure

The effect of water partial pressure on phenol conversion and H_2 yield as a function of S/C ratio is presented on Fig. 7a, with the equivalent partial pressure of water also annotated. For these experiments the total inlet flow (230 NmL min^{-1}), partial pressure of phenol (0.04 bar), and total pressure (1.9 bar) were kept constant while varying the partial pressure of water from 0.52 to 1.82 bar (balanced by N_2), which corresponds to a S/C variation from 2 to 7. On both catalysts, phenol conversion decreases with increasing water partial pressure, but with Rh activity being consistently higher than that of Ni-Co and the decrease of conversion being milder over Rh. These observations are confirmed further in Fig. 7b, where a negative reaction order on Ni-Co and a close to zero, but marginally negative, order on Rh with water partial pressure are obtained. Accounting for the positive order on phenol discussed in the previous section, results suggest that the rate controlling step lies on the phenol decomposition pathway. On the Ni-Co catalyst, competition

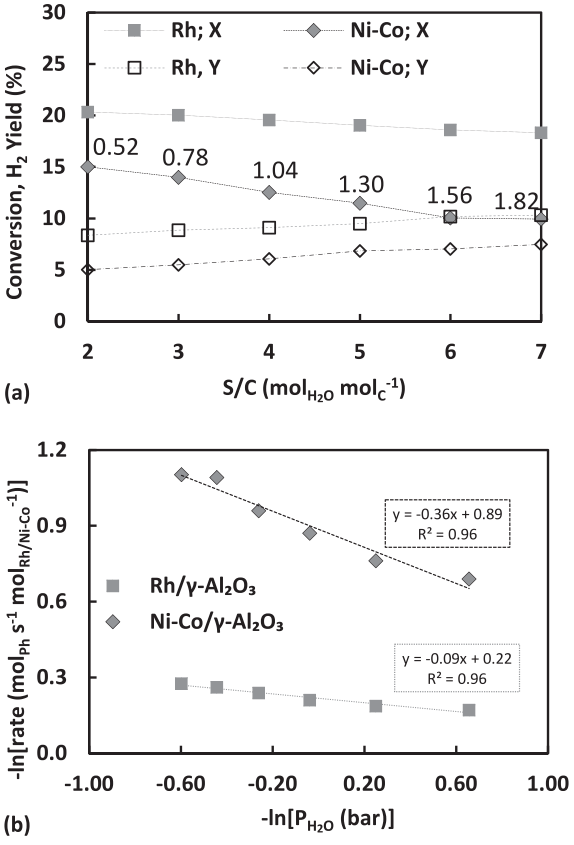

Fig. 7. Water partial pressure effect on phenol conversion (X) and H_2 yield (Y) on Rh and Ni-Co catalysts presented as a S/C variation with numbers on plot annotating the equivalent partial pressures of water in bar (a), and reaction order of PSR with respect to water partial pressures at 600 °C (b) (P = 1.9 bar, Q_{tot} = 230 NmL min^{-1}).

for active sites between water and phenol derivatives appears to be pronounced, whereas on Rh the steam-independent rate-limiting step proceeds largely unhindered. The differences between the two catalysts are possibly linked with the high oxophilicity of Co, which can lead to a preferential binding with oxygen surface species such as the OH groups from water. Nonetheless, the excess of water promotes the reforming and WGS reactions, with H_2 yield increasing from 8 % to 10 % on Rh and 5 % to 7 % on Ni-Co despite the concurrent drop in conversion. The impact of S/C ratio as observed in these experiments in comparison to that during the temperature variation experiments deserves also notice. Fig. 3 depicts an enhancement of phenol conversion with S/C, unlike results presented in Fig. 7a, however there are methodological differences that should be noted. Partial pressure variation experiments are carried out in a controlled manner to understand if water derived surface intermediates participate in the rate determining step. Temperature variation experiments are carried out at constant W/F_{Ph} and pressure (measured upstream of the catalyst bed). S/C variation impacts, hence, total space velocity, the partial pressures of both phenol and water, and pressure drop across the bed. As such, the two sets of experiments are not directly comparable. Moreover, S/C variation affects a range of reaction aspects, including the approach to equilibrium of parallel reactions, such as the water gas shift reaction. Indicatively, we have calculated the extent of the water–gas shift equilibrium ($\eta_{WGS} = P_{CO}\cdot P_{H_2O}/(P_{H_2}\cdot P_{CO_2}\cdot K_{WGS})$) under different reaction conditions. For all the partial pressure variation experiments, η_{WGS} remains approximately constant across each experiment ($\eta_{WGS}\approx1.5$ for Rh and P_{Ph} variation, $\eta_{WGS}\approx15$ for Ni-Co and P_{Ph} variation, $\eta_{WGS}\approx2.5$ for Rh and P_{H_2O} variation, $\eta_{WGS}\approx11$ for Ni-Co and P_{H_2O} variation). On the contrary, in the T variation data for 600 °C (the temperature at which P_i variation runs took place), η_{WGS} varies from 1 to 4 for Rh across the S/C = 2–9 range and from 3 to 11 for Ni-Co across the same S/C range. These data clearly indicate that, at least, the water gas shift reaction's approach to equilibrium is drastically different across similar S/C variations. This in turn can affect the surface coverage of CO, the latter being known to have a poisoning or inhibiting effect [69].

Fig. 8 presents the carbon selectivities of the products in terms of S/C ratio, with the equivalent water partial pressure values also annotated. Despite the decreasing trend of conversion, the selectivities of the products are exhibiting similar trends to those presented in the previous section. CO selectivity decreases from 60 % to 40 % on Ni-Co and from 43 % to 28 % on Rh, while CO_2 selectivity increases with higher water partial pressure. Rh presents higher WGS activity than the Ni-Co catalyst, with the CO/CO_2 ratio decreasing from 0.95 to 0.38 on the former, and from 2.37 to 0.71 on the latter as S/C increases, when thermodynamic equilibrium predicts CO/CO_2 values from 0.46 to 0.15 for the same S/C range. C_6H_6 and $C_{10}H_8$ selectivities both decrease as the partial pressure of water increases. As discussed in the introduction, the formation of CO_x during PSR requires the opening of the aromatic ring via C-C bond scission. The latter can take place either before or after O-H and/or C-O cleavage, but, in all cases, the very low C_6H_6 and $C_{10}H_8$ selectivities at S/C ratios over 5 indicates an effective conversion of the hydrocarbon fragments acting as precursors of these species through their reaction with hydroxyl groups [20].

3.5. Effect of space time

The effect of space time on phenol conversion and H_2 yield, at 600 °C and S/C of 2 and 7 over Rh and Ni-Co catalysts, is presented in Fig. 9. During these experiments the total reactants flow was modified over a fixed mass of catalyst with the space time varying from 59 to 293 g_{cat} s g_{Ph}^{-1}. As expected, for both catalysts, conversion and H_2 yield are increasing with space time and are enhanced with S/C ratio. Rh exhibits higher performance with conversion at 293 g_{cat} s g_{Ph}^{-1} being 9 % and 33 % at S/C of 2 to 7, with lower values of 7 % and 27 % reached on Ni-Co. H_2 yield similarly reaches 24 % on Rh at the highest S/C ratio and contact time, while only approaching 11 % on Ni-Co. Interestingly, for S/C of 7

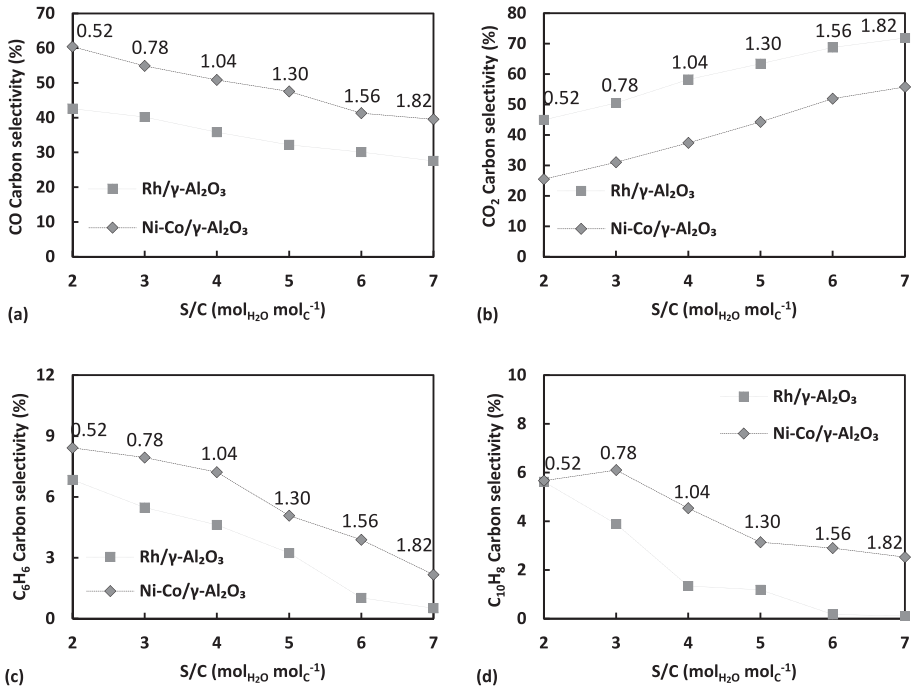

Fig. 8. Water partial pressure effect on carbon selectivities of CO (a), CO_2 (b), C_6H_6 (c) and $C_{10}H_8$ (d) on Rh and Ni-Co catalysts at 600 °C presented as a S/C variation with numbers on plot annotating the equivalent partial pressures of water in bar (P = 1.9 bar, Q_{tot} = 230 NmL min^{-1}).

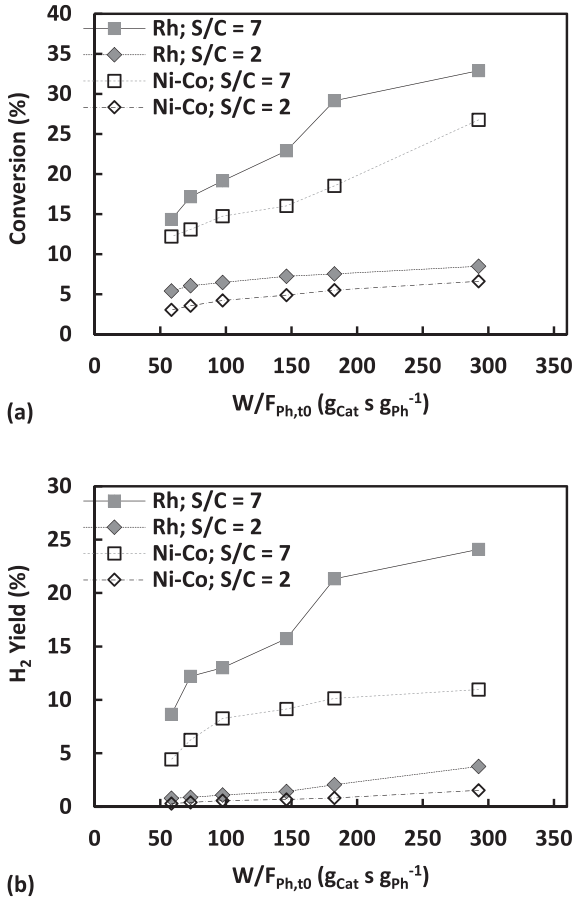

Fig. 9. $W/F_{Ph,t0}$ effect on phenol conversion (a) and H_2 yield (b) on Rh and Ni-Co catalysts at 600 °C (P = 1.8 bar, S/C = 2 or 7).

conversion on both catalysts increases more rapidly along with contact time, which indicates that the efficient oxidation of hydrocarbon and aromatic fragments by steam derived hydroxyls maintains the catalyst active sites free, allowing for reforming and WGS reactions to proceed more effectively. This beneficial effect of steam is further evidenced on the product selectivities discussed below.

On the Rh catalyst, for both S/C tested, CO and CO_2 selectivities show opposite trajectories against contact time, with that of CO approaching a finite value and that of CO_2 reaching a value of zero as conversion tends to zero (Fig. 10a and b). This implies the primary nature of CO, originating from the direct decomposition of phenol derived surface species. CO_2 is a secondary product of PSR formed from CO via the WGS reaction. For S/C of 2, CO selectivity is decreasing from 41 % to 27 % and that of CO_2 is increasing from 3 % to 49 %, while the conversion increases from 5 % to 9 %. The excess of water at S/C of 7 further enhances the WGS reaction with the CO_2 selectivity plateauing at almost 80 % as space time increases. At the highest contact time tested, the CO/CO_2 ratios obtained of 0.54 (S/C = 2) and 0.28 (S/C = 7) are close to those predicted by thermodynamic equilibrium 0.46 (S/C = 2) and 0.15 (S/C = 7) indicative that at adequate contact time the WGS reaction approaches equilibration despite the overall low conversions obtained. Increasing space time over Rh, C_6H_6 and $C_{10}H_8$ selectivities decrease for both S/C ratios tested (Fig. 10c and d), with that of benzene, and to a less extent of naphthalene, tending to zero rapidly at S/C of 2. The latter observation could however be affected by the low phenol conversion at this S/C, resulting in a progressively larger difficulty to quantify the aromatics. This impacts less the trends at S/C of 7, where the higher conversion achieved results in a smoother profile for both C_6H_6 and $C_{10}H_8$ selectivities that, nonetheless, decrease again to zero as space time increases. In all cases, the selectivity trajectories of C_6H_6 and $C_{10}H_8$ clearly indicate that both species are primary products over Rh.

Moderately different carbon selectivity profiles are observed on Ni-Co suggesting differences on the reaction pathway over this catalyst. For both S/C ratios tested, CO and CO_2 selectivities increase with contact time (Fig. 10a and b), whereas projecting their profiles to zero conversion indicates they would both reduce to zero. The trends suggest that over Ni-Co CO and CO_2 are secondary products, whose production is

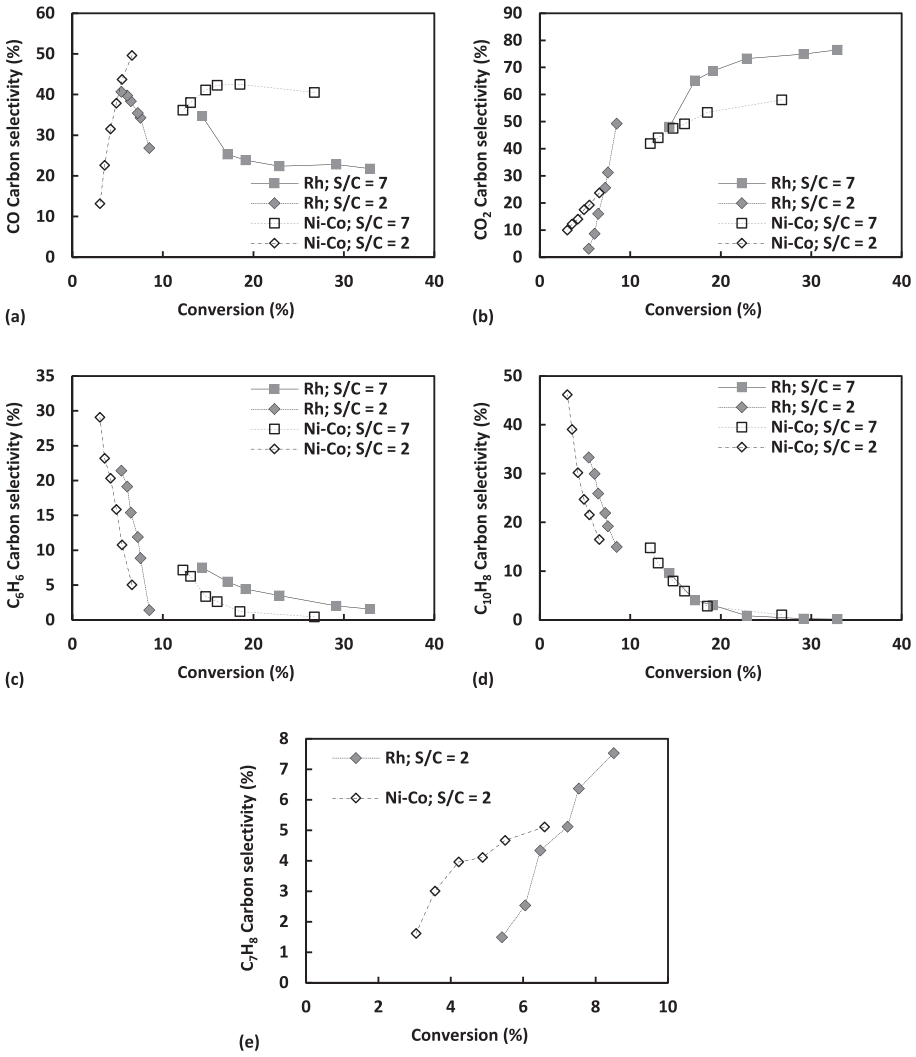

Fig. 10. Carbon selectivities of CO (a), CO_2 (b), C_6H_6 (c), $C_{10}H_8$ (d) and C_7H_8 (e) versus phenol conversion observed during $W/F_{Ph,t0}$ variation on Rh and Ni-Co catalysts at 600 °C (P = 1.8 bar, S/C = 2 or 7).

promoted by reforming and WGS reactions at high contact times and S/C. The best catalytic performance is obtained at S/C of 7 and at 293 g_{cat} s g_{Ph}^{-1}, where a CO/CO_2 ratio of 0.7, much lower than the equivalent value of 2.1 at S/C of 2, is achieved. In both cases, nonetheless, the values obtained are higher than those on Rh and those predicted by thermodynamic equilibrium. C_6H_6 and $C_{10}H_8$ (Fig. 10c and d) selectivities would have clearly finite values at zero conversion and are seen to decrease steadily with increase of conversion for both S/C ratios, evidence again that both compounds are primary products.

The detection of toluene at S/C of 2 is worthy to note (Fig. 10e), as the compound had not been detected during the experiments discussed in the previous sections. This difference can be attributed to the longer contact times studied in the present runs, as further supported by toluene's selectivity which increases with contact time (from 2 % to 8 % on Rh and from 1.5 % to 5 % on Ni-Co). Considering further that CH_4 was not detected at quantifiable concentrations throughout these experiments, the presence of methyl groups on the catalyst surface and the methylation rate of phenyl groups are expected to be low. As such, toluene's formation could be attributed to the reaction of benzene derived species with methylidene and methylidyne surface species, the latter formed via the decomposition of the aromatic ring. Based on the selectivity trend and the benzene-based formation pathway, toluene is a secondary product of PSR. No toluene was detected at S/C of 7, linked to the efficient reforming of toluene precursors, namely CH_x species, at excess water, but also to the much lower benzene selectivity at this S/C ratio.

3.6. Time-on-stream performance

Fig. 11 presents the evolution with time-on-stream on phenol conversion, H_2 yield and selectivities at 500 °C and a S/C of 2, examining the stability of both catalysts. On Rh, conversion shows a minor decrease from 17.6 % to 17 % in the 3-hour duration of the experiment, with H_2 yield averaging at 7 %. On Ni-Co, a relatively fast drop in conversion (from 16 to 14 %) occurs during the first hour, with catalytic performance stabilizing afterwards. H_2 yield follows this trend, decreasing from 7 to 5 % during the run. The drop in conversion over Ni-Co could indicate an initial blocking of active sites due to carbonaceous deposits build-up, with Ni widely known to suffer from coking in contrast to noble metals. Selectivity profiles show a decreasing trend for CO_2 and the opposite for CO, suggesting a gradual drop in WGS activity. Considering that the WGS is the terminal reaction in the PSR pathway, it is expected that catalyst deactivation would impact its progression first. The fact that Ni-Co is more affected compared to Rh further supports this. C_6H_6 selectivity is relatively high and remains almost stable at approximately 13 % on Ni-Co and 8 % on Rh. The higher value on the Ni-Co catalyst evidences again that this catalyst favours dehydroxylation reactions. Low $C_{10}H_8$ selectivity (<2%) is observed on both catalysts due

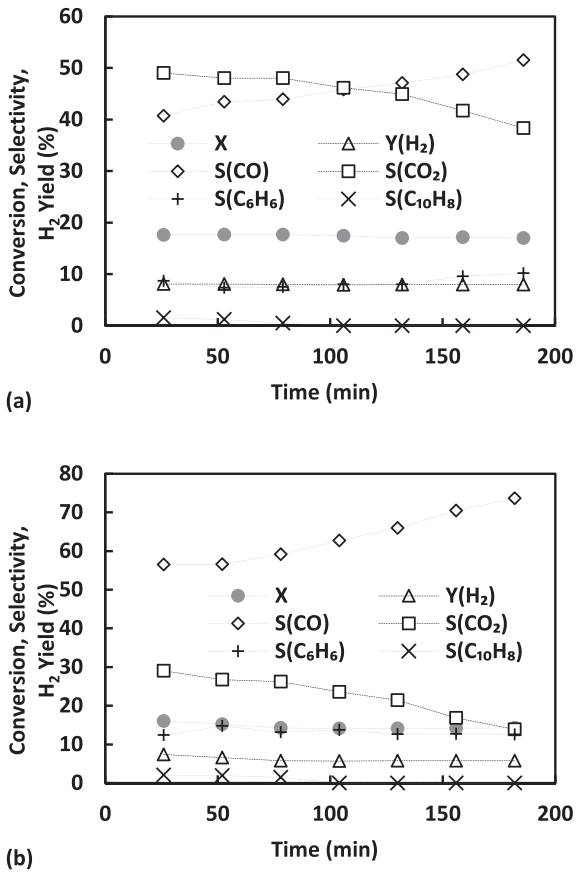

Fig. 11. Phenol conversion (X), H_2 yield (Y) and carbon selectivities (S) of CO, CO_2, C_6H_6 and $C_{10}H_8$ against time-on-stream on the Rh (a) and Ni-Co (b) catalysts at 500 °C (W/F_{Ph} = 487 g_{cat} s g_{Ph}^{-1}, S/C = 2).

to the relatively low operating temperature, which doesn't favour the decomposition reactions. Naphthalene's selectivity decreases with time, reaching zero at around 100 min, suggesting the blockage of certain active sites, due to coking, preventing $C_{10}H_8$ formation, or the shift towards graphitic carbon formation via polymerization and aromatic condensation reactions [70]. Nonetheless, the sharp drop of the selectivity to zero could also be affected by naphthalene's concentration falling below detection limits after a certain time on stream.

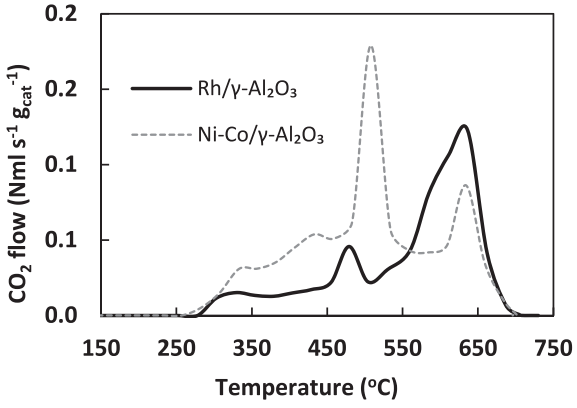

Fig. 12. CO_2 flow evolution during in situ coke oxidation of spent Rh and Ni-Co catalysts collected after 3 h time-on-stream experiments of phenol steam reforming at 500 °C and S/C = 2.

3.7. Temperature programmed oxidation of spent catalysts

The spent catalysts after the time-on-stream experiment were oxidised in situ to identify the amount and the type of carbon deposited. Fig. 12 presents the evolution of CO_2, while Table 2 presents the amount of carbon deposited on the catalyst bed. Three peaks at 320 °C, 490 °C and 640 °C were observed on the Rh catalyst, evidencing that carbon deposits of different nature are formed on the catalyst. The morphology and graphitisation degree of coke depends on feed, active metal, crystallite size and operating conditions [71]. Nonetheless, the peak at 320 °C indicates the formation of amorphous, highly reactive, coke, derived from decomposition and dehydrogenation reactions, while the peak at 490 °C suggests the formation of encapsulating coke derived from polymerization reactions. These types of coke can block the metal active sites; however, the relatively low size of these peaks agrees with the minor deactivation observed over Rh. The peak at 640 °C indicates the formation of carbon of graphitic nature produced from dehydrogenation reactions. These deposits are of filamentous/whisker structure [72] or possibly platelet/film morphology [73], given the low bulk diffusion of carbon in noble metals [71]. Moreover, they could be primarily forming on the support in line with the low carbon formation on this catalyst. As discussed in Section 3.1.1, the presence of residual chloride from the precursor is possible on the Rh catalyst. Cl^- ions are known to affect the acidity of the catalyst, which in turn impacts coke formation pathways [64]. For γ-Al_2O_3 based catalysts, residual chlorides are generally accepted to be associated with the support and not the metal [43,74], further suggesting that coke deposits on the Rh catalyst take place preferentially on the support and are not in contact with metal particles [64]. Results agree with studies on hydrocarbon oxidation and methane dry reforming over Rh based catalysts observing mainly graphitic carbon deposition and limited deactivation [75,76]. Regarding the Ni-Co catalyst, four peaks are observed at 330 °C, 440 °C, 480 °C and 640 °C, with the first three indicating the formation of amorphous and encapsulating carbon. In comparison with Rh, larger peaks are evident below approximately 550 °C suggesting a higher deactivation rate due to the formation of encapsulating carbon. A smaller peak at 640 °C indicates reduced formation of graphitic carbon on Ni-Co. Thermodynamic equilibrium predicts the formation of graphitic carbon only at sub-stoichiometric S/C ratio (Figure S3, SI), however, over both catalysts, it is evident that there are kinetic pathways, possibly support-mediated, that lead to the formation of such deposits. Further characterisation techniques, such as Raman spectroscopy and HRTEM, would be required to provide more information of the type and location of coke deposits present on spent samples and whether on the Rh catalyst these deposits are linked to the presence of residual Cl^- ions on the support [64,74]. Almost 50 % higher carbon deposition is observed on the Ni-Co catalyst in comparison to Rh (Table 2). Overall, the time-on-stream results and the lower carbon deposition on the Rh catalyst compared to the Ni-Co catalyst clearly highlight the higher catalytic performance of the Rh catalyst for the phenol reforming reaction both in terms of activity but also stability.

4. Discussion

Fig. 13 depicts schematically the proposed phenol steam reforming reaction pathways over Rh and Ni-Co catalysts, in line with the experimental observations of this work. Based on DFT calculations [30] and

Table 2
Mass-based percentages of carbon deposited as coke on catalyst samples in terms of carbon fed and catalyst mass after 3 h time-on-stream experiments of phenol steam reforming at 500 °C and S/C = 2.

Catalyst sample	Coke/Carbon fed (%)	Coke/Catalyst mass (%)
Rh/γ-Al_2O_3	0.6	9.9
Ni-Co/γ-Al_2O_3	0.9	14.8

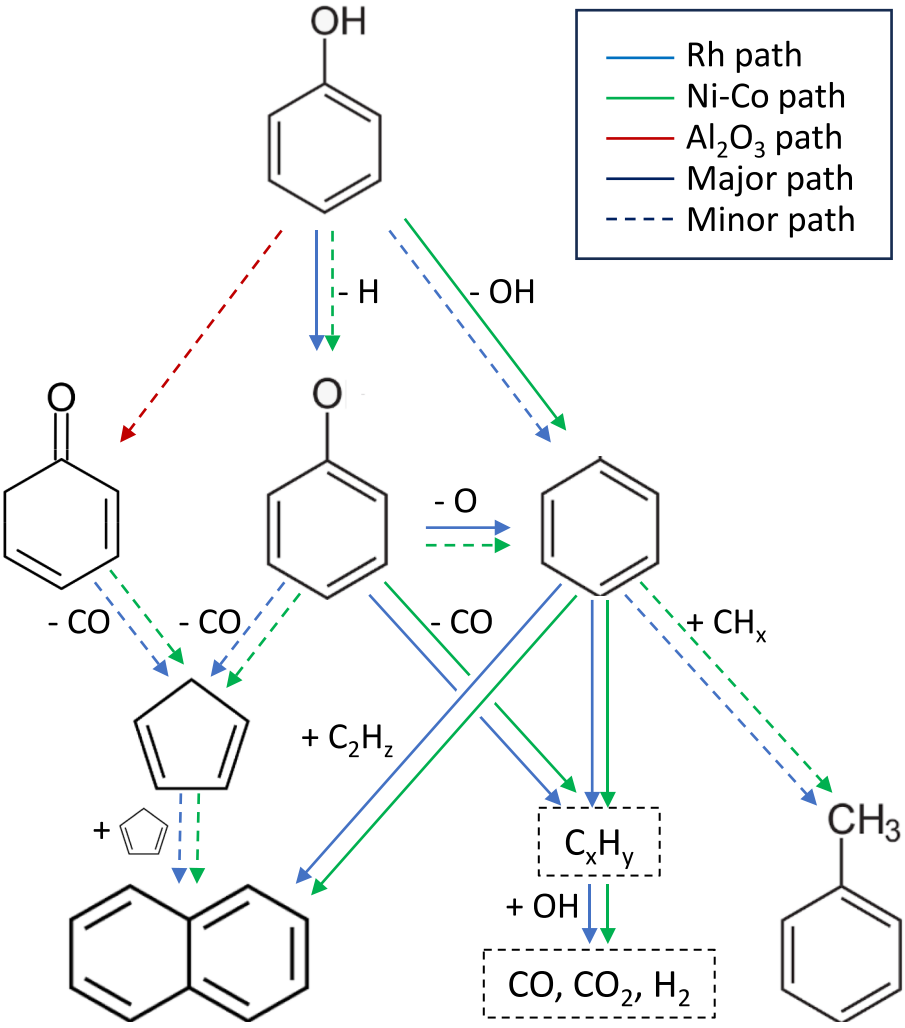

Fig. 13. Proposed reaction pathways of phenol steam reforming on Rh and Ni-Co catalysts. Blue, green, and red arrows indicate pathways that take place on the Rh metal particle, Ni-Co metal particle, and γ-Al_2O_3 support, respectively. Major and minor paths per catalyst are indicated with solid and dashed lines, respectively. (For interpretation of the references to colour in this figure legend, the reader is referred to the web version of this article.)

experimental studies [29] on phenol reactivity over Rh(1 1 1), phenol is suggested to adsorb with the aromatic ring parallel to the catalyst surface, followed by phenoxy species formation via O-H bond scission. Phenoxy species further decompose stoichiometrically over Rh flat surfaces, forming CO with the C-O bond remaining intact [29], a pathway that aligns with CO having been identified as a primary product over this catalyst. DFT calculations and experimental studies on HDO of anisole have alternatively suggested that over Rh stepped metal sites phenoxy species could be hydrodeoxygenated to benzene following a cleavage of the C-O bond [77]. This parallel pathway over low-coordination sites of the Rh catalyst particles would be responsible for benzene also being a primary product of PSR, although the possibility of subsequent C–O bond cleavage of phenoxy species cannot be eliminated. Gas phase studies have discussed the decomposition of phenoxy species to CO and cyclopentadienyl radicals [78], with the latter also possibly being present on the catalyst surface constituting naphthalene's precursor via its dimerization [62]. Phenol's decomposition could also proceed through its tautomerization to cyclohexadienone over acid sites of the support, however, as discussed, this pathway appears to be limited at our conditions. Nonetheless, cyclohexadienone's further decomposition to CO and cyclopentadienyl radicals [79] could be a contributing mechanism towards naphthalene. In all cases, the opening of the aromatic ring of either phenoxy species formed via O-H scission or phenyl species formed via eventual C-O scission leads to the presence of C_xH_y species on the catalyst surface. As discussed also in various studies on toluene steam reforming over Rh catalysts, these hydrocarbon fragments react with water derived hydroxyls to eventually produce CO_x and H_2 [80,81]. Hydroxyl species possibly result from water's dissociation on the support, spilling over to the metal particles [20], which aligns with the observed kinetic independence of PSR on water partial pressure.

Over Ni-Co, phenol also adsorbs horizontally [65], however, the reaction network initiates with C-O bond scission, due to cobalt's higher oxophilicity, which, as already described, favours dehydroxylation. This pathway is further consistent with CO being identified as a secondary product over this catalyst. Phenoxy species formation cannot be dismissed, however it would similarly be followed by C-O bond cleavage towards phenyl formation. In line with benzene being a primary product, phenyl species can hydrogenate to benzene [82], also justifying the latter's higher selectivity on this catalyst. These observations further agree with HDO phenol studies over Ni bimetallic catalysts suggesting that the addition of Co increased the selectivity towards the deoxygenation reactions, while Ni was more active in hydrogenation reactions, favouring benzene formation [83]. Phenyl species undergo successive C-C bond cleavages, producing C_xH_y species, which can be oxidised to CO_x with steam-derived hydroxyls. The higher oxophilicity of this catalyst is potentially responsible for the stronger binding of hydroxyl groups, resulting in the observed negative reaction order with water. Hydrocarbon fragments can further react with phenyl groups towards

naphthalene, in line with gas phase studies having demonstrated the addition of acetylene to phenyl towards naphthalene formation [84,85]. Cyclopentadienyl dimerization would be less prominent over this catalyst, as CO is not expected to be extracted intact from phenol.

On both catalysts, increasing the contact time enhances CO_2 and H_2 production via reforming and WGS reactions, while phenyl reactions with CH_x species at low S/C ratios and long contact times promote the formation of toluene.

Time-on-stream experiments indicated the stable performance of the catalysts, although a gradual impact on selectivities was noticed. TPO analysis of spent samples evidenced the formation of coke deposits, suggesting that deactivation of the catalysts would occur over time. Sintering of metal particles would also be possible after extended operation at high temperature. The location of coke, the ability of the catalyst to oxidise coke deposits via efficient OH supply and extent of sintering would determine deactivation rates [6], although any impact on kinetics and dominant reaction pathways would merit independent study.

5. Conclusions

The steam reforming of phenol was examined over Rh and Ni-Co catalysts supported on γ-Al_2O_3 to assess the effect of operating conditions and metal on the reaction mechanism. The study revealed a range of differences in the reaction pathways over the two catalysts that were rationalised based on the oxophilicity of the metals, namely cobalt's higher affinity to the oxygen-containing hydroxyl groups of phenol and water. A positive reaction order on phenol for Rh and Ni-Co suggested the strong adsorption of the aromatic on both catalyst surfaces, while a negative order in water over Ni-Co, in contrast to near steam-independent kinetics on Rh, indicated the stronger binding of hydroxyls groups on Ni-Co. On Rh, the reaction mechanism initiates with the O-H bond cleavage, forming phenoxy surface species, whereas on Ni-Co, the reaction network proceeds with C-O bond scission or O-H cleavage followed by C-O bond scission, forming phenyl intermediate species. In support of this mechanism, CO was found to be a primary product over Rh evidencing it is extracted intact during phenoxy decomposition, in contrast to Ni-Co where the same compound was a secondary product. Benzene, a major product on both catalysts, showed higher selectivity on Ni-Co on account of enhanced C-O bond scission and phenyl formation on that catalyst. Comparing the catalytic performance of both catalysts it was observed that Rh was the most active presenting higher conversion, syngas formation and stability, while exhibiting significantly lower carbon formation.

CRediT authorship contribution statement

Marinela D. Zhurka: Writing – original draft, Investigation. **Alan J. McCue:** Resources, Writing – review & editing. **Panagiotis N. Kechagiopoulos:** Conceptualization, Methodology, Writing – review & editing, Supervision.

Declaration of competing interest

The authors declare that they have no known competing financial interests or personal relationships that could have appeared to influence the work reported in this paper.

Data availability

Data will be made available on request.

Acknowledgement

Professor Angeliki Lemonidou from the Aristotle University of Thessaloniki is gratefully acknowledged for hosting MZ and assisting with catalyst preparation.

Appendix A. Supplementary data

Supplementary data to this article can be found online at https://doi.org/10.1016/j.fuel.2024.131102.

References

[1] Abou Rjeily M, Gennequin C, Pron H, Abi-Aad E, Randrianalisoa JH. Pyrolysis-catalytic upgrading of bio-oil and pyrolysis-catalytic steam reforming of biogas: a review. Environ Chem Lett 2021;19:2825–72.
[2] Shao S, Zhang P, Li X, Yu Y. Steam reforming of the simulated aqueous fraction of bio-oil based on pre-reforming with dolomite. Fuel 2023;344:128116.
[3] Abdelaal A, Antolini D, Piazzi S, Patuzzi F, Villot A, Gerente C, et al. Steam reforming of tar using biomass gasification char in a Pilot-scale gasifier. Fuel 2023;351:128898.
[4] Kong G, Liu Q, Ji G, Jia H, Cao T, Zhang X, et al. Improving hydrogen-rich gas production from biomass catalytic steam gasification over metal-doping porous biochar. Bioresour Technol 2023;387:129662.
[5] Wang Y, Lu Z, Chen M, Liang D, Wang J. Hydrogen production from catalytic steam reforming of toluene over trace of Fe and Mn doping Ni/Attapulgite. J Anal Appl Pyrolysis 2022;165:105584.
[6] Charisiou ND, Polychronopoulou K, Asif A, Goula MA. The potential of glycerol and phenol towards H_2 production using steam reforming reaction: A review. Surf Coat Technol 2018;352:92–111.
[7] Li J, Wang C, Yang Z. Production and separation of phenols from biomass-derived bio-petroleum. J Anal Appl Pyrolysis 2010;89:218–24.
[8] Gowthami R, Sharpudin J. Removal of phenol from textile wastewater using natural adsorbent. Int J Sci Eng Technol Res 2016;5:2278–7798.
[9] Saleem M. Pharmaceutical wastewater treatment: A physicochemical study. J Res Sci 2007;18:125–34.
[10] Nabgan W, Abdullah TAT, Mat R, Nabgan B, Gambo Y, Johari A. Evaluation of reaction parameters of the phenol steam reforming over Ni/Co on ZrO_2 using the full factorial experimental design. Appl Sci 2016;6:1–21.
[11] Matas Güell B, Babich IV, Lefferts L, Seshan K. Steam reforming of phenol over Ni-based catalysts - A comparative study. Appl Catal B 2011;106:280–6.
[12] Baamran KS, Tahir M. Steam reforming of phenol toward cleaner hydrogen production over bimetallic Ni/Ti modified zinc titanate perovskite in tandem with a kinetic model development. J Clean Prod 2021;311:127519.
[13] Meng J, Zhao Z, Wang X, Chen J, Zheng A, Huang Z, et al. Steam reforming and carbon deposition evaluation of phenol and naphthalene used as tar model compounds over Ni and Fe olivine-supported catalysts. J Energy Inst 2019;92:1765–78.
[14] Koike M, Li D, Watanabe H, Nakagawa Y, Tomishige K. Comparative study on steam reforming of model aromatic compounds of biomass tar over Ni and Ni-Fe alloy nanoparticles. Appl Catal A Gen 2015;506:151–62.
[15] Saeed Baamran K, Tahir M. Thermodynamic investigation and experimental analysis on phenol steam reforming towards enhanced H_2 production over structured Ni/$ZnTiO_3$ nanocatalyst. Energy Convers Manag 2019;180:796–810.
[16] Artetxe M, Nahil MA, Olazar M, Williams PT. Steam reforming of phenol as biomass tar model compound over Ni/Al_2O_3 catalyst. Fuel 2016;184:629–36.
[17] Garbarino G, Lagazzo A, Riani P, Busca G. Steam reforming of ethanol-phenol mixture on Ni/Al_2O_3: Effect of Ni loading and sulphur deactivation. Appl Catal B 2013;129:460–72.
[18] Chitsazan S, Sepehri S, Garbarino G, Carnasciali MM, Busca G. Steam reforming of biomass-derived organics: Interactions of different mixture components on Ni/Al_2O_3 based catalysts. Appl Catal B 2016;187:386–98.
[19] Xu Y, Zhu Y, Shen P, Chen G, Li X. Production of hydrogen by steam reforming of phenol over Ni/Al_2O_3-ash catalysts. Int J Hydrogen Energy 2022;47:13592–603.
[20] Polychronopoulou K, Costa CN, Efstathiou AM. The steam reforming of phenol reaction over supported-Rh catalysts. Appl Catal A Gen 2004;272:37–52.
[21] Mosayebi A. The kinetic and experimental study of the phenol steam reforming towards hydrogen production over Ni-Rh/MgO catalyst. Fuel 2023;334:126711.
[22] Li P, Li X, Wang Y, Shen P, Zhu X, Zhu Y, et al. Low-temperature steam reforming of phenol for hydrogen production over Co/Al_2O_3–ash catalysts. Appl Catal B 2022;316:121691.
[23] Wang C, Wang Y, Chen M, Liang D, Cheng W, Li C, et al. Hydrogen production from tar steam reforming over hydrangea-like Co-phyllosilicate catalyst derived from Co/Sepiolite. Int J Hydrogen Energy 2023;48:2542–57.
[24] Liang D, Wang Y, Chen M, Xie X, Li C, Wang J, et al. Dry reforming of methane for syngas production over attapulgite-derived MFI zeolite encapsulated bimetallic Ni-Co catalysts. Appl Catal B 2023;322:122088.
[25] Nabgan W, Tuan Abdullah TA, Mat R, Nabgan B, Triwahyono S, Ripin A. Hydrogen production from catalytic steam reforming of phenol with bimetallic nickel-cobalt catalyst on various supports. Appl Catal A Gen 2016;527:161–70.
[26] Abbas T, Tahir M. Tri-metallic Ni–Co modified reducible TiO_2 nanocomposite for boosting H_2 production through steam reforming of phenol. Int J Hydrogen Energy 2021;46:8932–49.
[27] Russell JN, Saks SS, Morris RE. Adsorption and thermal decomposition of phenol on Ni(110). Surf Sci 1995;338:189–203.
[28] Teles CA, Rabelo-Neto RC, Jacobs G, Davis BH, Resasco DE, Noronha FB. Hydrodeoxygenation of phenol over zirconia-supported catalysts: The effect of

metal type on reaction mechanism and catalyst deactivation. ChemCatChem 2017; 9:2850–63.
[29] Xu X, Friend CM. Role of coverage in determining adsorbate stability: Phenol reactivity on Rh(111). J Phys Chem 1989;93:8072–80.
[30] Honkela ML, Björk J, Persson M. Computational study of the adsorption and dissociation of phenol on Pt and Rh surfaces. Phys Chem Chem Phys 2012;14: 5849–54.
[31] Garcia-Pintos D, Voss J, Jensen AD, Studt F. Hydrodeoxygenation of phenol to benzene and cyclohexane on Rh(111) and Rh(211) surfaces: Insights from density functional theory. J Phys Chem C 2016;120:18529–37.
[32] Mahboob S, Haghighi M, Rahmani F. Sonochemically preparation and characterization of bimetallic Ni-Co/Al_2O_3-ZrO_2 nanocatalyst: Effects of ultrasound irradiation time and power on catalytic properties and activity in dry reforming of CH_4. Ultrason Sonochem 2017;38:38–49.
[33] Torres D, Pinilla JL, Suelves I. Co-, Cu-and Fe-doped Ni/Al_2O_3 catalysts for the catalytic decomposition of methane into hydrogen and carbon nanofibers. Catalysts 2018;8:1–15.
[34] Chen X, Honda K, Zhang ZG. CO_2-CH_4 reforming over NiO/γ-Al_2O_3 in fixed-bed/ fluidized-bed switching mode. Catal Today 2004;93–95:87–93.
[35] Ji L, Tang S, Zeng HC, Lin J, Tan KL. CO_2 reforming of methane to synthesis gas over sol-gel-made Co/γ-Al_2O_3 catalysts from organometallic precursors. Appl Catal A Gen 2001;207:247–55.
[36] Zhang J, Wang H, Dalai AK. Development of stable bimetallic catalysts for carbon dioxide reforming of methane. J Catal 2007;249:300–10.
[37] Moodley DJ, Saib AM, Van De Loosdrecht J, Welker-Nieuwoudt CA, Sigwebela BH, Niemantsverdriet JW. The impact of cobalt aluminate formation on the deactivation of cobalt-based Fischer-Tropsch synthesis catalysts. Catal Today 2011; 171:192–200.
[38] Hwang CP, Yeh CT, Zhu Q. Rhodium-oxide species formed on progressive oxidation of rhodium clusters dispersed on alumina. Catal Today 1999;51:93–101.
[39] Oliveira RL, Bitencourt IG, Passos FB. Partial oxidation of methane to syngas on Rh/Al_2O_3 and Rh/Ce-ZrO_2 catalysts. J Braz Chem Soc 2013;24:68–75.
[40] Goula G, Botzolaki G, Osatiashtiani A, Parlett CMA, Kyriakou G, Lambert RM, et al. Oxidative thermal sintering and redispersion of Rh nanoparticles on supports with high oxygen ion lability. Catalysts 2019;9:541–57.
[41] Montini T, Condò AM, Hickey N, Lovey FC, De Rogatis L, Fornasiero P, et al. Embedded Rh(1 wt.%)@Al2O3: Effects of high temperature and prolonged aging under methane partial oxidation conditions. Appl Catal B 2007;73:84–97.
[42] Samoila P, Epron F, Marécot P, Especel C. Influence of chlorine on the catalytic properties of supported rhodium, iridium and platinum in ring opening of naphthenes. Appl Catal A Gen 2013;462–463:207–19.
[43] Kip BJ, Dirne FWA, van Grondelle J, Prins R. The effect of chlorine in the hydrogenation of carbon monoxide to oxygenated products at elevated pressure on Rh and Ir on SiO_2 and Al_2O_3. Appl Catal 1986;25:43–50.
[44] Narita T, Miura H, Ohira M, Hondou H, Sugiyama K, Matsuda T, et al. The effect of reduction temperature on the chemisorptive properties of Ru/Al_2O_3: Effect of chlorine. Appl Catal 1987;32:185–90.
[45] Shirasuka K, Yanagida H, Yamaguchi G. The Preparation of η-Alumina and Its Structure. J Ceram Soc Jpn 1976;84:610–3.
[46] Liu X, Prewitt CT. High-temperature X-ray diffraction study of Co_3O_4: Transition from normal to disordered spinel. Phys Chem Miner 1990;17:168–72.
[47] O'Neill HSC. Temperature dependence of the cation distribution in $CoAl_2O_4$ spinel. Eur J Mineral 1994;6:603–10.
[48] O'Neill HSC, Dollase WA, Ross CR. Temperature dependence of the cation distribution in nickel aluminate (NiAl2O4) spinel: a powder XRD study. Phys Chem Miner 1991;18:302–19.
[49] Lambert TN, Vigil JA, White SE, Davis DJ, Limmer SJ, Burton PD, et al. Electrodeposited $Ni_xCo_3-xO_4$ nanostructured films as bifunctional oxygen electrocatalysts. Chem Commun 2015;51:9511–4.
[50] Cairns RW, Ott E. X-Ray Studies of the System Nickel-Oxygen-Water. I. Nickelous Oxide and Hydroxide. J Am Chem Soc 1933;55:527–33.
[51] Biesterbos JWM, Hornstra J. The crystal structure of the high-temperature, low-pressure form of Rh_2O_3. J Less-Common Met 1973;30:121–5.
[52] Shirako Y, Wang X, Tsujimoto Y, Tanaka K, Guo Y, Matsushita Y, et al. Synthesis, crystal structure, and electronic properties of high-pressure PdF2-Type Oxides MO2 (M = Ru, Rh, Os, Ir, Pt). Inorg Chem 2014;53:11616–25.
[53] Huang C, Ma Z, Miao C, Yue Y, Hua W, Gao Z. Catalytic decomposition of N_2O over Rh/Zn-Al_2O_3 catalysts. RSC Adv 2017;7:4243–52.
[54] Cheng CK, Lim RH, Ubil A, Chin SY, Gimbun J. Hydrogen as carbon gasifying agent during glycerol steam reforming over bimetallic Co-Ni catalyst. Adv Mater Sci Eng 2012;2:165–8.
[55] Siang TJ, Singh S, Omoregbe O, Bach LG, Phuc NHH, Vo DVN. Hydrogen production from CH_4 dry reforming over bimetallic Ni–Co/Al_2O_3 catalyst. J Energy Inst 2018;91:683–94.
[56] Peres APS, Lima AC, Barros BS, Melo DMA. Synthesis and characterization of $NiCo_2O_4$ spinel using gelatin as an organic precursor. Mater Lett 2012;89:36–9.
[57] Thimthong N, Appari S, Tanaka R, Iwanaga K, Namioka T, Kudo S, et al. Numerical study on the steam reforming of biomass tar using a detailed chemical kinetic model. J Jpn Inst Energy 2015;94:794–804.
[58] Arandia A, Remiro A, García V, Castaño P, Bilbao J, Gayubo AG. Oxidative steam reforming of raw bio-oil over supported and bulk Ni catalysts for hydrogen production. Catalysts 2018;8:322–47.
[59] Ceriotti A, Martinengo S, Zanderighi L, Tonelli C, Iannibello A, Girelli A. Use of supported rhodium and cobalt carbonyls as catalysts for the CO + H2 reaction. Effect of the support and the metal. J Chem Soc 1984;80:1605–16.
[60] Miyazaki E. Chemisorption of Diatomic Molecules (H2, N2, CO) on Transition d-Metals. J Catal 1980;94:84–94.
[61] Tan Q, Wang G, Long A, Dinse A, Buda C, Shabaker J, et al. Mechanistic analysis of the role of metal oxophilicity in the hydrodeoxygenation of anisole. J Catal 2017; 347:102–15.
[62] Mebel AM, Landera A, Kaiser RI. Formation mechanisms of naphthalene and indene: From the interstellar medium to combustion flames. J Phys Chem A 2017; 121:901–26.
[63] Wei J, Iglesia E. Structural requirements and reaction pathways in methane activation and chemical conversion catalyzed by rhodium. J Catal 2004;225: 116–27.
[64] Angeli SD, Turchetti L, Monteleone G, Lemonidou AA. Catalyst development for steam reforming of methane and model biogas at low temperature. Appl Catal B 2016;181:34–46.
[65] Site LD, Alavi A, Abrams CF. Adsorption energies and geometries of phenol on the (111) surface of nickel: An ab initio study. Phys Rev B 2003;67:1–3. 193406.
[66] Orita H, Itoh N. Simulation of phenol formation from benzene with a Pd membrane reactor: ab initio periodic density functional study. Appl Catal A Gen 2004;258: 17–23.
[67] Bonalumi N, Vargas A, Ferri D, Baiker A. Theoretical and spectroscopic study of the effect of ring substitution on the adsorption of anisole on platinum. J Phys Chem B 2006;110:9956–65.
[68] Carlos H-T, Roldan A, De LNH. Tautomerization of phenol at the external Lewis acid sites of Sc-, Fe- and Ga-substituted zeolite MFI. J Phys Chem C 2019;123: 7604–14.
[69] Kandoi S, Greeley J, Simonetti D, Shabaker J, Dumesic JA, Mavrikakis M. Reaction kinetics of ethylene glycol reforming over platinum in the vapor versus aqueous phases. J Phys Chem C 2011;115:961–71.
[70] Granda M, Blanco C, Alvarez P, Patrick JW, Menéndez R. Chemicals from coal coking. Chem Rev 2014;114:1608–36.
[71] Helveg S, Sehested J, Rostrup-Nielsen JR. Whisker carbon in perspective. Catal Today 2011;178:42–6.
[72] Chiodo V, Freni S, Galvagno A, Mondello N, Frusteri F. Catalytic features of Rh and Ni supported catalysts in the steam reforming of glycerol to produce hydrogen. Appl Catal A Gen 2010;381:1–7.
[73] Sasson Bitters J, He T, Nestler E, Senanayake SD, Chen JG, Zhang C. Utilizing bimetallic catalysts to mitigate coke formation in dry reforming of methane. J Energy Chem 2022;68:124–42.
[74] Vasiliadou ES, Heracleous E, Vasalos IA, Lemonidou AA. Ru-based catalysts for glycerol hydrogenolysis—Effect of support and metal precursor. Appl Catal B 2009; 92:90–9.
[75] Smith MW, Shekhawat D, Berry DA, Haynes DJ, Floyd DL, Spivey JJ, et al. Carbon formation on Rh-substituted pyrochlore catalysts during partial oxidation of liquid hydrocarbons. Appl Catal A Gen 2015;502:96–104.
[76] Pakhare D, Wu H, Narendra S, Abdelsayed V, Haynes D, Shekhawat D, et al. Characterization and activity study of the Rh-substituted pyrochlores for CO2 (dry) reforming of CH4. Appl Petrochem Res 2013;3:117–29.
[77] Duong NN, Aruho D, Wang B, Resasco DE. Hydrodeoxygenation of anisole over different Rh surfaces. Chinese J Catal 2019;40:1721–30.
[78] Nowakowska M, Herbinet O, Dufour A, Glaude PA. Kinetic study of the pyrolysis and oxidation of guaiacol. J Phys Chem A 2018;122:7894–909.
[79] Xu ZF, Lin MC. Ab initio kinetics for the unimolecular reaction C6H5OH → CO + C5H6. J Phys Chem A 2006;110:1672–7.
[80] Duprez D, Miloudi A, Delahay G, Maurel R. Selective steam reforming of aromatic hydrocarbons. VI. Steam conversion and hydroconversion of selected monoalkyl- and dialkylbenzenes on Pt and Ni catalysts. J Catal 1986;101:56–66.
[81] Grenoble DC. The chemistry and catalysis of the water/toluene reaction 2. The role of support and kinetic analysis. J Catal 1978;51:212–20.
[82] Bui VN, Laurenti D, Afanasiev P, Geantet C. Hydrodeoxygenation of guaiacol with CoMo catalysts. Part I: Promoting effect of cobalt on HDO selectivity and activity. Appl Catal B 2011;101:239–45.
[83] Huynh TM, Armbruster U, Pohl MM, Schneider M, Radnik J, Hoang DL, et al. Hydrodeoxygenation of phenol as a model compound for bio-oil on non-noble bimetallic nickel-based catalysts. ChemCatChem 2014;6:1940–51.
[84] Chu TC, Buras ZJ, Smith MC, Uwagwu AB, Green WH. From benzene to naphthalene: Direct measurement of reactions and intermediates of phenyl radicals and acetylene. Phys Chem Chem Phys 2019;21:22248–58.
[85] Moldoveanu SC. Pyrolysis of hydrocarbons. Pyrolysis of organic molecules. Elsevier; 2019. p. 35–161.